Proc. R. Soc. Lond. B **228**, 379–400 (1986)
Printed in Great Britain

The structure and symmetry of simple-cell receptive-field profiles in the cat's visual cortex

By D. J. Field and D. J. Tolhurst

Department of Physiology, University of Cambridge, Downing Street, Cambridge CB2 3EG, U.K.

(*Communicated by F. W. Campbell, F.R.S. – Received* 24 *October* 1985)

Receptive fields of simple cells in the cat visual cortex have recently been discussed in relation to the 'theory of communication' proposed by Gabor (1946). A number of investigators have suggested that the line-weighting functions, as measured orthogonal to the preferred orientation, may be best described as the product of a Gaussian envelope and a sinusoid (i.e. a Gabor function). Following Gabor's theory of 'basis' functions, it has also been suggested that simple cells can be categorized into even- and odd-symmetric categories.

Based on the receptive field profiles of 46 simple cells recorded from cat visual cortex, our analysis provides a quantitative description of both the receptive-field envelope and the receptive-field 'symmetry' of each of the 46 cells. The results support the notion that, to a first approximation, Gabor functions with three free parameters (envelope width, carrier frequency and carrier phase) provide a good description of the receptive-field profiles. However, our analysis does not support the notion that simple cells generally fit into even- and odd-symmetric categories.

Introduction

Early studies of the receptive-field properties of neurons in the mammalian visual cortex were primarily restricted to analyses in terms of spatially localized stimuli such as edges and bars (see, for example, Hubel & Wiesel 1962). This 'space domain' approach was later supplemented by the 'frequency domain' or 'Fourier' approach (see, for example, Cooper & Robson 1968; Campbell, *et al.* 1969; Maffei & Fiorentini 1973; Ikeda & Wright 1975). In this second form of analysis, receptive fields are described in terms of their response to sinusoidal gratings as a function of the grating's spatial frequency, phase and orientation. The general approach has been given wide support in the psychophysical literature and has served as the basis of a general theory of vision which proposes that the visual system analyses spatial information into its Fourier components (see, for example, Campbell & Robson 1968; Blakemore & Campbell 1969; Ginsburg 1971; Weistein & Bisaha 1972; Maffei & Fiorentini 1973; Albrecht *et al.* 1979).

However, it has been widely suggested that a complete theory of spatial vision must involve a compromise between the two approaches (see, for example, Glezer *et al.* 1973; Robson 1980; Marcelja 1980; Kulikowski & Bishop 1981*a*). Cells of the

visual cortex respond selectively to *both* limited bands of spatial frequencies and to local regions of space. Therefore, both position (space domain) and spatial frequency information may be provided by such cells.

This compromise between position and spatial frequency is reminiscent of Gabor's (1946) discussion of the analysis of signals which change with time. Indeed, it has recently been suggested that the line-weighting functions of simple cells, as measured orthogonal to the preferred orientation, may be best described (or modelled) in terms of Gabor's 'elementary signals', often called 'Gabor functions' (Marcelja 1980; Kulikowski & Bishop 1981*a*; Sakitt & Barlow 1982; Kulikowski *et al.* 1982; Watson 1983). A 'Gabor function' is the product of a Gaussian envelope and a sinusoid:

$$R(x) = \exp[-(x-x_0)^2/2\sigma^2]\cos[2\pi f(x-x_0)-\theta]. \quad (1)$$

The phase (θ), the spatial frequency (f) and the width of the envelope (σ) may take on any values while remaining within the general definition of a 'Gabor function'. Figure 1 shows Gabor functions for a variety of phases and for two

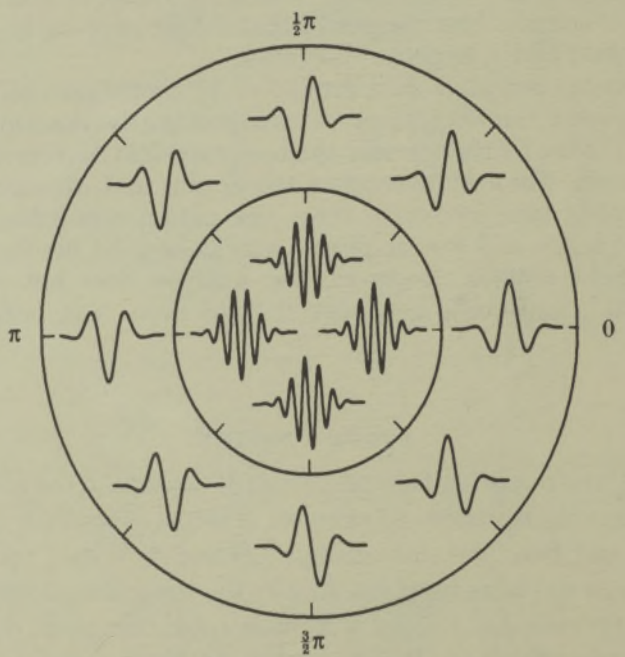

FIGURE 1. A polar plot of theoretical Gabor functions. All functions shown have the same Gaussian envelope. The phase of the function, as shown on the outside edge, follows (1). The inner and outer set of functions show two carrier frequencies.

carrier frequencies. All these examples have the same Gaussian envelope. The interest in such functions arises partly because Gabor's (1946) theory suggests that such functions are ideally suited for the compromise between locating the position of a signal in space and for identifying the spatial frequency of the signal. But even if one does not accept the notion that the frequency-selective properties play a major role in visual perception, Gabor functions may provide a convenient three-parameter description of the receptive-field profiles.

However, although there have been suggestions that the line-weighting functions of simple cells resemble the general shape of Gabor functions, there has yet to be any quantitative evidence to support such a hypothesis. The first goal of this paper is to determine the extent to which the line-weighting functions can be described by Gabor functions. (It has been suggested that the profiles along the axis of the preferred orientation may also be described by Gabor functions (see, for example, Kulikowski *et al.* 1982; Daugman 1981; Palmer *et al.* 1985). However, our discussion will be restricted to the one-dimensional profile as revealed by the line-weighting function.)

The second issue addressed by this paper involves the question of whether these functions can generally be described as either even symmetric ($R(-x) = R(x)$) or odd symmetric ($R(-x) = -R(x)$). In terms of Gabor functions, even-symmetric functions will have a phase (θ in equation 1) of either 0 or π (see figure 1 for example). Odd-symmetric functions have a phase of either $\frac{1}{2}\pi$ or $\frac{3}{2}\pi$. Gabor functions with other phases would be neither even nor odd symmetric (e.g. $\theta = \frac{1}{4}\pi$ in figure 1).

Several investigators have suggested that the line-weighting functions are at least generally even or odd symmetric (Movshon *et al.* 1978; Kulikowski & Bishop 1981*a*,*b*; Pollen & Ronner 1981; Kulikowski *et al.* 1982; Maske *et al.* 1985). However, as with the notion that simple cells resemble Gabor functions, there is no quantitative physiological evidence to support such an hypothesis.

It should be noted, however, that there exists psychophysical (i.e. behavioural) evidence along these lines. Although such results are by no means conclusive, several investigators (including the authors) have suggested that their behavioural data can be accounted for by assuming only even- and odd-symmetric mechanisms (Kulikowski & Kingsmith 1973; Tolhurst & Dealy 1975; Field & Nachmias 1984).

The advantages of paired even- and odd-symmetric functions have been discussed previously (Gabor 1946; Marcelja 1980; Kulikowski & Bishop 1981*b*; Pollen & Ronner 1981). A pair of such functions with the same orientation and frequency tuning centred at the same point in space are orthogonal and could serve as a 'basis set'; they are theoretically sufficient to identify the phase and amplitude of the signal at that point.

However, any two Gabor functions that differ in phase by $\frac{1}{2}\pi$ (e.g. $\theta = \frac{1}{4}\pi$ and $\theta = \frac{3}{4}\pi$) will fulfil the requirements of orthogonal elementary signals. They need not be even and odd symmetric. Pollen & Ronner have shown that many pairs of adjacent simple cells differ in phase by 90° ($\frac{1}{2}\pi$). This result is consistent with the hypothesis that pairs of simple cells may serve as 'elementary signals'. However, their results do not imply that the receptive fields must be even and odd symmetric. This issue will be discussed in greater detail later.

Thus the second section of this paper is devoted to a quantitative analysis of the line-weighting functions of simple cells to determine whether they fit within the even- and odd-symmetric categories or whether they fit within any orthogonal groups.

Methods

The methods of recording, experimental design and data analysis have been reported in detail elsewhere (Movshon *et al.* 1978; Tolhurst & Thompson 1981; Dean & Tolhurst 1983). The data reported in this paper were collected as parts of these earlier projects.

Preparation and recording

Neurons were recorded in area 17 of adult cats using conventional techniques. During the experiments, the cats were anaesthetized by hyperventilating them with a mixture of N_2O:O_2:CO_2 (75:23:1.5); the gas was supplemented by IV infusion of sodium pentobarbitone (0.5–1.5 mg kg^{-1} h^{-1}). The cats were paralysed with an infusion of gallamine triethiode (10 mg kg^{-1} h^{-1}). The adequacy of anaesthesia was determined from continuous monitoring of the electroencephalogram and heart rate (see Dean & Tolhurst 1986). End-tidal CO_2 concentration was maintained at 4–5% by adjustment of stroke volume. Rectal temperature was maintained at 37–38 °C. The eyes were protected with zero-power contact lenses, opaque except for a central 3 mm transparent aperture. At the end of the experiments, the cats were given an overdose of barbiturates.

The recordings were made with tungsten-in-glass micro-electrodes (Levick 1972; Merrill & Ainsworth 1972). Electrode penetrations were made into that part of area 17 representing the central 5° of the visual field.

Experiments

For each neuron, the non-dominant eye was covered. Receptive fields of neurons were initially mapped using hand-controlled spots or lines of light projected onto a flat-tangent screen 114 cm from the cat's eyes. The aims were to determine the extent of the visual field in which responses were evoked when the stimuli were flashed on and off and to determine whether the receptive field comprised discrete ON and OFF regions. The optimal stimulus orientation was also determined. The experimenter assessed the neuron's response by listening to an audiomonitor of the electrode recording.

The receptive fields of all 46 neurons described in this paper were mapped quantitatively (Movshon *et al.* 1978). None of these was end inhibited. The luminance of a raster display screen was locally varied to create optimally orientated thin bright and dark lines, of rectangular luminance profile. The space-averaged luminance of the raster, generated on a P-31 phosphor was, for different cats, 150–450 cd m^{-2}. This value is well within the photopic range when seen through the 3 mm artificial pupil which was used (Daw & Pearlman 1970). The stimuli were either flashed on and off at 1 Hz or (more usually) modulated sinusoidally in luminance at the same temporal frequency. The lines were presented in various positions in and around the receptive field and the line width was chosen so that the field was covered by six to twelve lines. The luminance of the lines was usually 1.5 times (bright) or 0.5 times (dark) the luminance of the rest of the raster. The response to each line was averaged over 30–100 stimulus cycles.

Results

The 46 cells described in this paper were classed as simple cells (Hubel & Weisel 1962). Their receptive fields comprised relatively discrete excitatory and inhibitory regions. The widths of these regions were approximately half the period of the optimal spatial frequency of a sinusoidal grating (Dean & Tolhurst 1983).

Figure 2*a* shows the quantitative receptive field map (the line-weighting function) for one of the neurons. The histogram shows the amplitude of response to optimally oriented lines presented in several locations within the receptive field. The choice of line positions was such that neighbouring lines would have been exactly adjacent, without overlap. Line width was chosen so that each region was covered by two or three lines; this resulted in line-weighting functions comprising from six to twelve lines (Dean & Tolhurst 1983). The width of the histogram blocks in figure 2*a* represents the width of the lines used for creating the map. The response to a bright line is considered to be positive, while the response to a dark line is considered to be negative. In some cells, both bright and dark lines elicited a response at a single receptive field location (Movshon *et al.* 1978; Dean & Tolhurst 1983): then, the value plotted is the difference between the responses to the two polarities of line. One could argue that removing the overlap by taking the difference between responses will result in an incomplete description of the receptive-field profile. It is a matter that deserves attention and it points out the limitations in analysing the response properties of these cells in terms of a single continuous function. Unfortunately, for those cells which show overlap, there seems to be little alternative to taking the difference. Without such a procedure, the analyses described in this paper would not be possible.

The neuron illustrated in figure 2*a* has a receptive field which comprises one strong excitatory region and one strong inhibitory region. It may be that this receptive field can be described as the product of an envelope ($f(x)$) and a sinewave:

$$R(x) = f(x)\cos(2\pi fx - \theta). \tag{2}$$

The objects of this paper are to examine the structure of the receptive-field envelopes, $f(x)$, and to examine the distribution of θ in the population of neurons.

Discrete Fourier transform

As shown by the line-weighting functions on the top of figure 2, our methods produce a 'quantized' version of the actual receptive field profile. The discrete steps in the function are due to the finite size of the bars and not to the underlying receptive field. To remove these steps, we performed a discrete Fourier transform on each of the line-weighting functions. Figure 2 shows the result of such a process.

As for each of the 46 neurons, the line-weighting function was analysed into ten equally spaced frequencies ranging from one twentieth to one half the sampling frequency (sampling frequency = 1/barwidth); the highest frequency in the discrete Fourier transform is limited by the sampling theorem to one half the sampling frequency. This transform results in amplitude spectra and phase spectra like those shown in figure 2*b*, *c* (the phase spectra will be discussed in detail later).

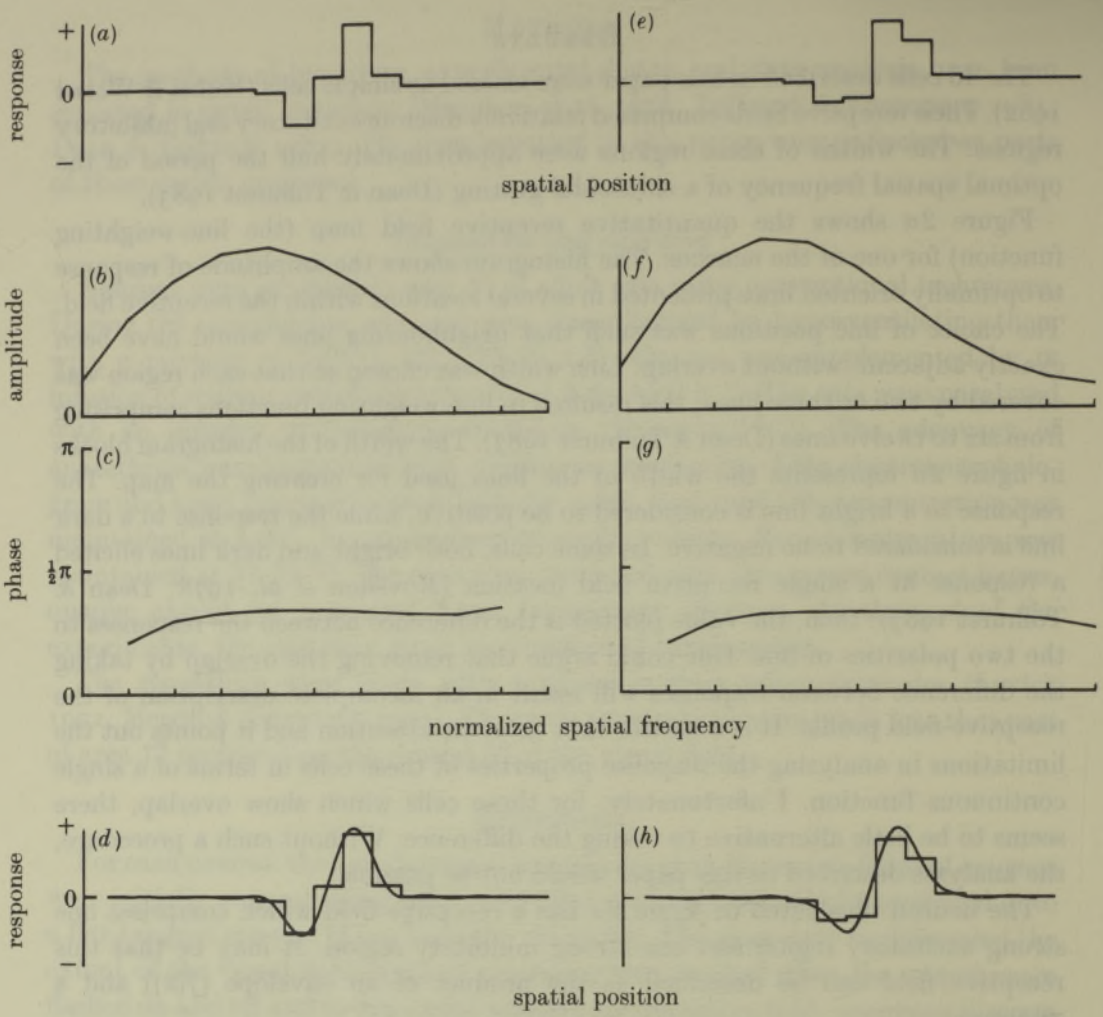

FIGURE 2. Discrete Fourier transform. The top lines (*a*) and (*e*), show two line-weighting functions obtained with the same cell. The function in (*e*) was obtained with bars positioned ½ of a bar width to the right of the positions in (*a*). The amplitude spectra, (*b*) and (*f*), and the phase spectra, (*c*) and (*g*) of these two line-weighting functions are also shown. The spectra consist of ten equally spaced frequencies with the highest frequency equal to ½ the sampling frequency. The smooth curves on the bottom line, (*d*) and (*h*) show the estimated receptive field profiles based on the inverse Fourier transform of these spectra. We refer to the spatial frequency as 'normalized' because the range of frequencies is completely determined by the spacing between the bars (i.e. the bar width). For this particular cell, the bar width is 0.19°. This results in a spectrum with ten frequencies ranging from 0.263 up to 2.63 cycles deg^{-1}. However, since the bar width varied from cell to cell, the precise range covered by these ten frequencies was not constant.

Adding these ten frequencies with their appropriate amplitudes and phases (inverse Fourier transform) provides our estimate of the underlying receptive-field profile. Figure 2*d* shows the line-weighting function for the cell along with the estimate derived from the discrete Fourier transform.

It should be noted that frequencies higher than one half the sampling frequency are obscured by this process. That is, the width and the distance between the bars

makes it impossible to resolve any high frequency content in the receptive-field profile. However, for most cells, the amplitude spectrum was approaching zero at the high frequency limit (as shown in figure 2*b*) which suggests that little if any information is lost by this process. None the less, it should be noted that errors in the spectra can be introduced by these methods. Although we feel that our conclusions are unaffected by the magnitude of these errors, we provide a more thorough discussion in Appendix 1.

Theoretically, this method should provide an accurate estimate of the receptive-field profile which is independent of the original sampling positions of the bars. To demonstrate this, we show results when the receptive field was mapped again with the bars in different positions. Figure 2*e* shows the line-weighting function when the lines were shifted one half a linewidth to the left of the positions shown in figure 2*a*. As one might expect, the line-weighting functions appear substantially different. However, the amplitude spectra (figure 2*b*, *f*) and phase spectra (figure 2*c*, *g*) derived from these two line-weighting functions are quite satisfyingly similar. And, as predicted, the estimated receptive fields from each of the line-weighting functions are quite comparable.

Receptive-field envelopes

As noted earlier, it has been suggested that receptive fields of simple cells are best fitted by the general equation:

$$R(x) = \exp[-(x-x_0)^2/2\sigma^2]\cos[2\pi f(x-x_0)-\theta]. \quad (1)$$

All functions that fit this equation have, by definition, a Gaussian envelope. In this section we determine whether the envelopes of our receptive fields are Gaussian.

There exists a standard method for estimating a function's envelope, i.e. for extracting the modulating waveform from an amplitude-modulated signal. The general approach was referred to by Gabor (1946) and is discussed in more detail by Bracewell (1965) and de Weerd & Kap (1981).

Consider the two functions shown on the top of figure 3: these are the receptive field profiles of two neurons estimated from the discrete Fourier transform. Each function is represented by the following:

$$R(x) = \sum_n a_n \cos(2\pi f_n - \theta_n), \quad (3)$$

where a_n and θ_n are the amplitude and phase of the nth frequency (f_n).

To estimate the envelope of each function, it is first necessary to calculate each function's Hilbert transform (Bracewell 1965). This is simply a phase-shifted version of the original function:

$$H(R(x)) = \sum_n a_n \cos(2\pi f_n x - \theta_n + \tfrac{1}{2}\pi). \quad (4)$$

The functions on the second row show the Hilbert transforms of the two top functions. At each point in space, a function and its Hilbert transform can be

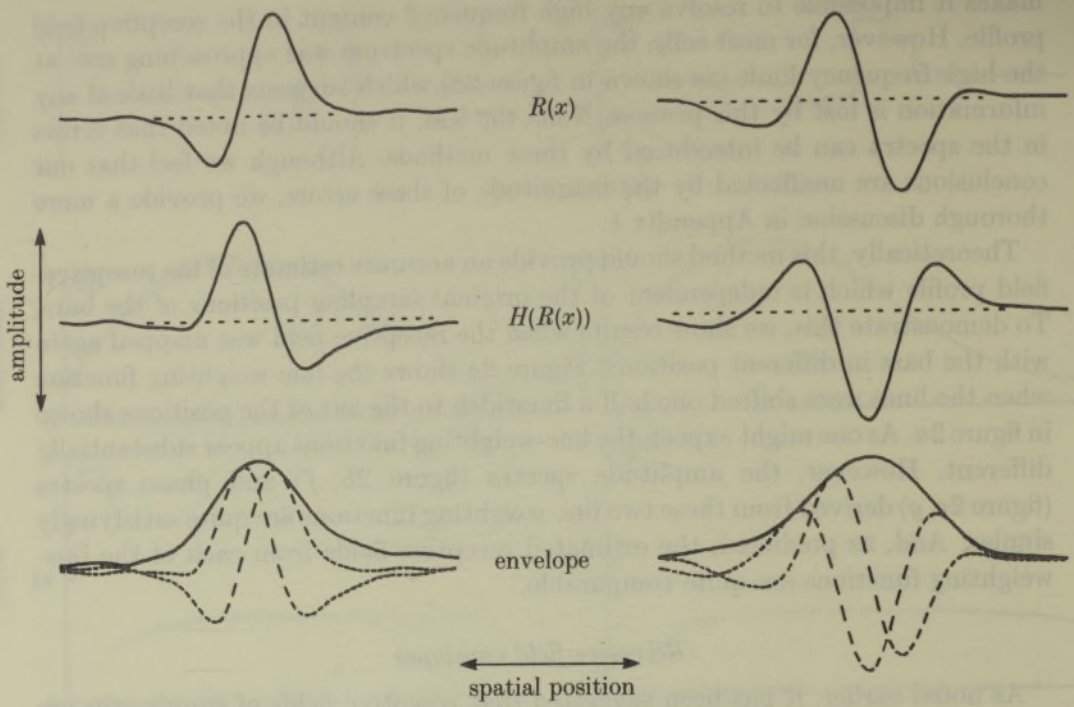

FIGURE 3. The figures on the top row show two receptive-field profiles, $R(x)$, resulting from the discrete Fourier transform. The second row, $H(R(x))$, shows the Hilbert transforms of these two profiles. The bottom row shows the envelopes (solid lines) of the two receptive-field profiles along with the profile and its Hilbert transform (dashed lines).

described as representing orthogonal vectors. The envelope is the vector sum of these two vectors:

$$E(x) = \sqrt{[R(x)^2 + H(R(x))^2]}. \tag{5}$$

The bottom row of figure 3 shows the envelopes of the two receptive-field profiles (solid lines) along with the profile and its Hilbert transform (dashed lines).

Estimates of the receptive-field envelope were made for each of the 46 cells and the results are shown in figure 4. Because we are interested only in the overall shape of the envelope and not on its size, each envelope has been normalized to the same height and half-width. One can see that the shape of all the envelopes remains fairly consistent. They have their greatest amplitude near the centre and they decay more or less symmetrically on each side. They mostly resemble Gaussians.

The average of these 46 normalized envelopes is shown in figure 5*a*. Note the small standard deviation around this average. A Gaussian of the same width and height is also shown (dashed line). It closely resembles the averaged envelope.

Figure 5*b* shows how well each envelope is fitted by a Gaussian. For each envelope, the best fitting Gaussian was found by a least-squares criterion. The normalized residual variance, V_r is given by:

$$V_r = \sum_x (E(x) - G(x))^2 / \sum_x (E(x) - \bar{E})^2, \tag{6}$$

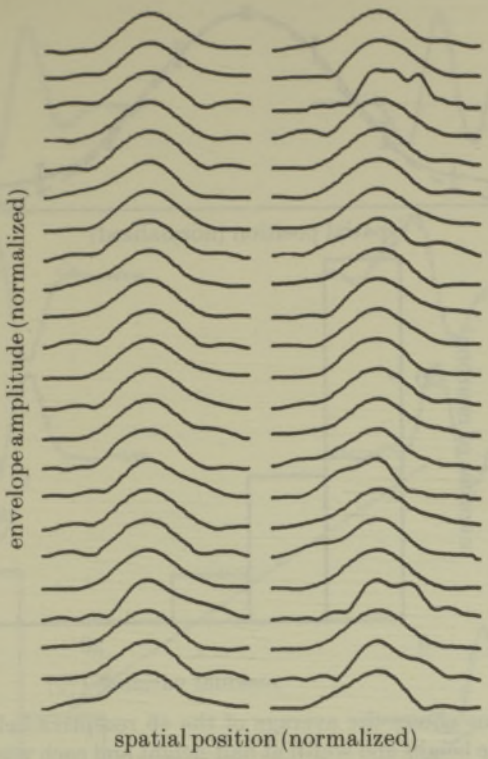

FIGURE 4. The estimated envelopes of the 46 receptive-field profiles. Because we are not interested in the overall size of the envelope but just its shape, each envelope has been normalized to the same height and to the same width at half-height.

where $E(x)$ is the amplitude of the envelope and $G(x)$ is the amplitude of the best fitting Gaussian. As one can see, for most of the neurons, the residual variance was less than 5 %. In other words, for these 30 cells, more than 95 % of the envelope variance can be accounted for by the best fitting Gaussian. There are few marked deviations.

Gabor functions

The results of this analysis suggest that, to a first approximation the envelopes of these cells can be described as having a Gaussian profile. But does this imply that the receptive fields themselves are Gabor functions?

To answer this question we determined the optimal phase and frequency that produced the best fitting Gabor function. That is, we began with the best fitting Gaussian envelope, as determined above. Then by means of an iterative search through possible phases (θ) and frequencies (f) we found the Gabor function that produced the smallest residual variance (V_r). The results of this analysis are shown in figure 6.

The histogram on the bottom of figure 6, shows the goodness of fit for each of the 46 cells. Also shown are examples of estimated receptive fields (solid lines) and the best fitting Gabor function (dotted lines). The results show that for 30 out of

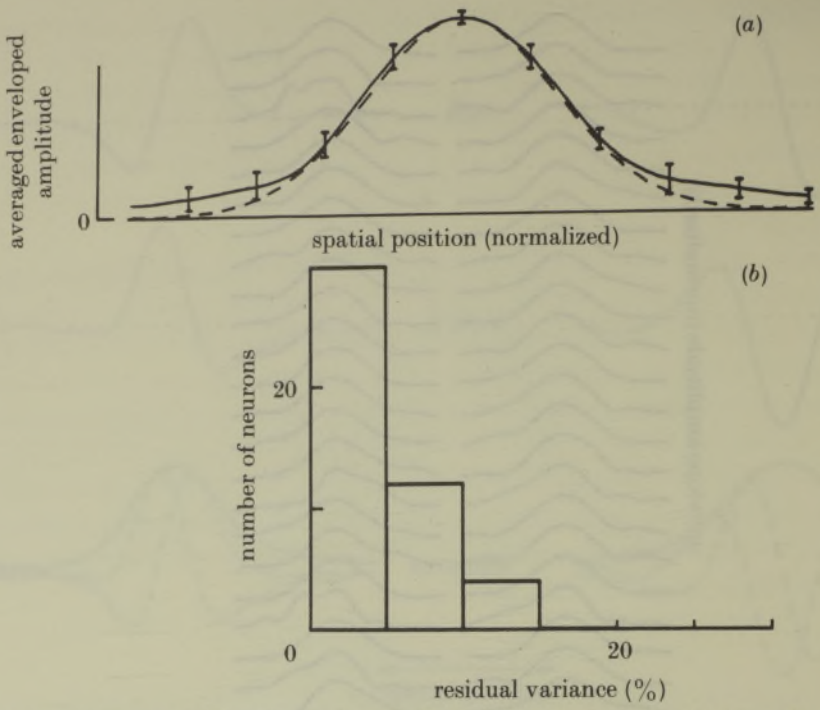

FIGURE 5. (*a*) The solid line shows the average of the 46 receptive-field envelopes. Each was normalized to the same height and width at half-height and each was positioned at the same centre of mass. Error bars are ± 1 s.d. The dashed line shows a true Gaussian. (*b*) The histogram shows the 'goodness of fit' of a Gaussian to each of the 46 receptive field envelopes. The normalized residual variance, V_r is defined in the text.

46 cells, the best fitting Gabor function could account for more than 95% of the variance in the receptive-field profiles. Again, there are few marked deviations.

These results suggest that most simple cell receptive-field profiles are reasonably described by Gabor functions.

Receptive-field symmetry

In this section, we consider whether receptive-field profiles fall into distinct even-symmetric ($\theta = 0$ or π) and odd-symmetric ($\theta = \frac{1}{2}\pi$ or $\frac{3}{2}\pi$) classes. The first approach is to consider the values of θ obtained by finding the best fitting Gabor function (above).

As was shown in figure 1, it is theoretically possible for θ to vary from 0 to 2π. However, in practice, we must limit our discussion to the range of 0 to π. Consider an odd-symmetric receptive-field profile with $\theta = \frac{1}{2}\pi$ (i.e. excitation on the left and inhibition on the right). Such a profile is derived from a cell with some preferred orientation (e.g. vertical). Rotating the two-dimensional profile through 180° (in orientation) will result in a profile of $\theta = \frac{3}{2}\pi$ (i.e. inhibition on the left and excitation on the right). In other words, the distinction between profiles with $\theta > \pi$ from profiles with $\theta < \pi$, is confounded by an absolute definition of orientation.

Since the neurons in this study had a wide variety of preferred stimulus

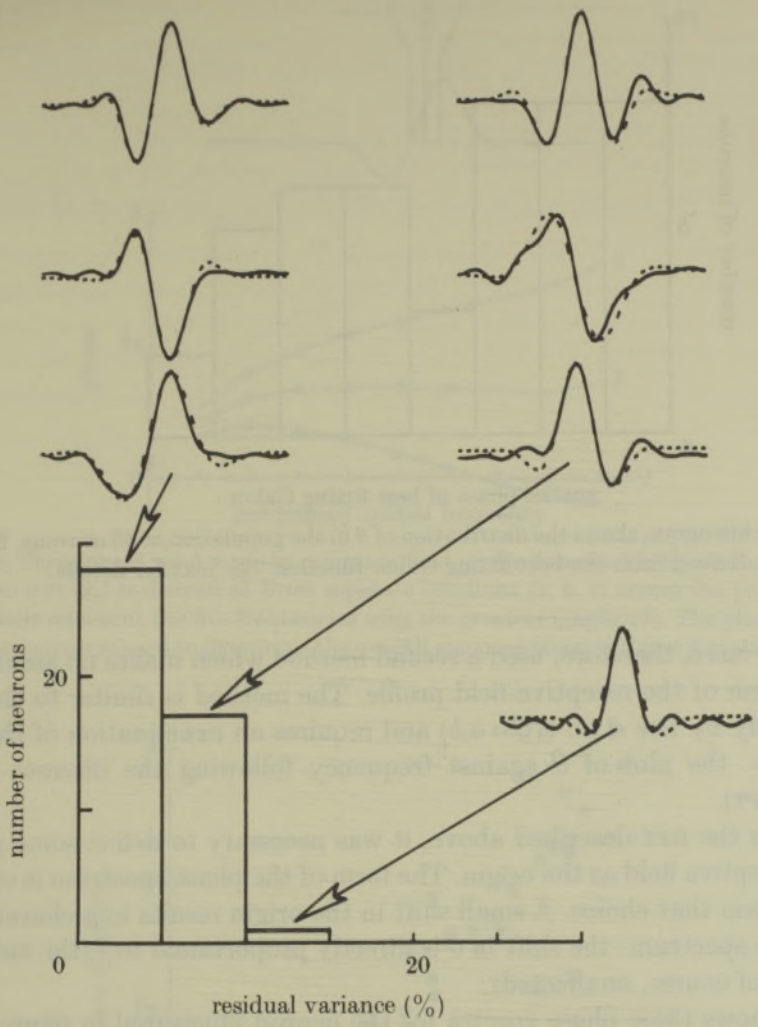

FIGURE 6. The histogram shows the 'goodness of fit' of the best fitting Gabor function to each of the 46 receptive-field profiles. The normalized residual variance V_r, is defined in the text. Also shown are several examples of the profiles (solid lines) and the Gabor functions (dashed lines) that correspond to the different degrees of fit.

orientations, an absolute definition of orientation would be meaningless. Hence, our discussion of θ must be limited to the range of 0 to π. If, from the analysis, θ was found to fall between π and 2π, it was reflected (about π) to fall in the range of 0 to π (i.e. $\theta = \pi + x$ becomes $\theta = \pi - x$). This process has no effect on our ability to assess whether receptive fields fall into distinct even- and odd-symmetric classes.

Figure 7 shows the distribution of θ in the population of the 46 neurons. It is clear that there is no grouping near values of 0 and π (even symmetric) or near $\frac{1}{2}\pi$ (odd symmetric). Nor is any other orthogonal grouping clearly evident; the values are distributed almost uniformly across the spectrum.

It may be argued that this method of estimating θ is too artificial and presumes that the receptive-field profile conforms to a particular structure, i.e. a Gabor

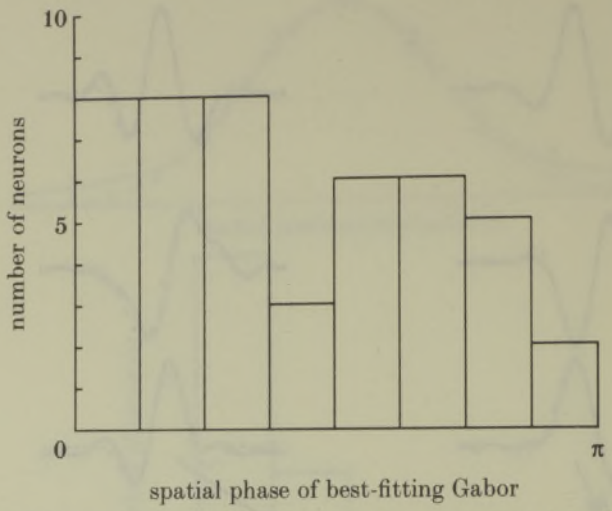

FIGURE 7. The histogram shows the distribution of θ in the population of 46 neurons. Estimates are derived from the best fitting Gabor function. See text for details.

function. We have, therefore, used a second method which makes no assumptions about the form of the receptive-field profile. The method is similar to that used experimentally by Lee *et al.* (1981*a*,*b*) and requires an examination of the phase spectrum (i.e. the plot of θ against frequency following the discrete Fourier transform, DFT).

To perform the DFT described above, it was necessary to define some position along the receptive field as the origin. The form of the phase spectrum is critically dependent upon that choice. A small shift in the origin results in a characteristic change in the spectrum: the shift in θ is directly proportional to f (the amplitude spectrum is, of course, unaffected).

Figure 8 shows three phase spectra for the neuron illustrated in figure 2 after the DFT was performed with three slightly different origins. The goal of this analysis is to assign to each neuron a *single* value of θ. Hence, an origin is selected which results in a phase spectrum whose slope is zero. That is, θ is the Y-intercept of the best fitting horizontal line. Thus, for each cell, we systematically varied the origin for performing the DFT until the phase spectrum was best fit by a horizontal line. We considered only the phases of the five frequencies with the highest amplitudes; at the extremes of the spectrum, where the amplitudes are low and little different from the 'noise', the phase may vary randomly.

The results of this analysis were similar to those obtained by estimating the phase of the best-fitting Gabor function. Figure 9 plots the two estimates of phase against each other. There is a linear relation with a high correlation ($r = 0.97$). This more empirical analysis confirms that there is no predominance of even- and odd-symmetric receptive-field profiles.

The results of this analysis were also found to provide further support for the notion that the receptive-field profiles can be likened to Gabor functions. For many kinds of function, it is not possible to define an origin which results in a horizontal phase spectrum. However, within certain constraints (see Appendix 2), Gabor functions are one class of function for which this is possible. When the five

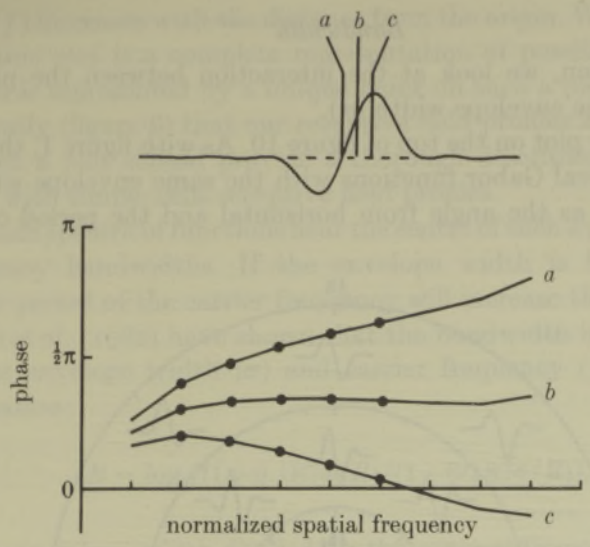

FIGURE 8. Three phase spectra of the receptive-field profile described in figure 2, when the origin of the DFT (x_0) is defined at three separate locations (a, b, c) across the profile. The filled symbols represent the five frequencies with the greatest amplitude. The phase at these five frequencies was used to determine the overall response phase in figure 9 (i.e. unconstrained).

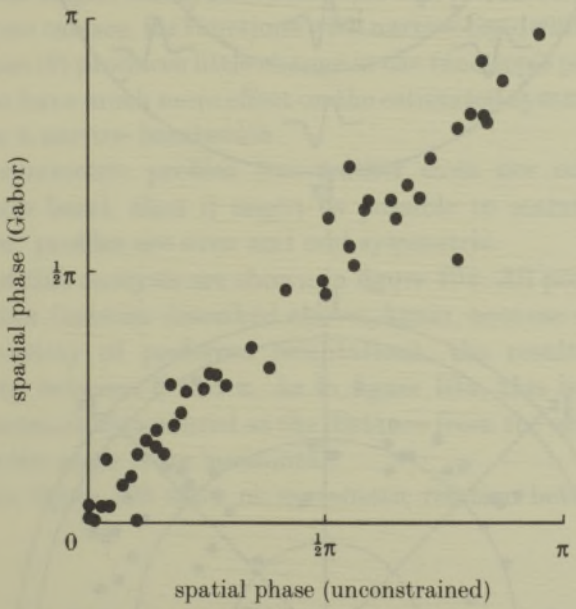

FIGURE 9. Estimates of θ derived from the best-fitting Gabor function plotted against the estimates derived from the unconstrained phase spectra ($r = 0.97$).

frequencies of highest amplitude were considered, the neurons in our sample *did* show remarkably flat phase spectra (e.g. figure 8). We determined the standard deviation of θ about the mean for the five frequency components. For 27 of the 46 neurons, this was less than $\frac{1}{50}\pi$ (i.e. 3.6°) and for only 3 neurons was it greater than $\frac{1}{25}\pi$ (7.2°).

Bandwidth

In this final section, we look at the interaction between the phase (θ), the frequency (f) and the envelope width (σ).

Consider the polar plot on the top of figure 10. As with figure 1, this plot shows a variety of theoretical Gabor functions with the same envelope width (σ). The phase (θ) is plotted as the angle from horizontal and the period of the carrier

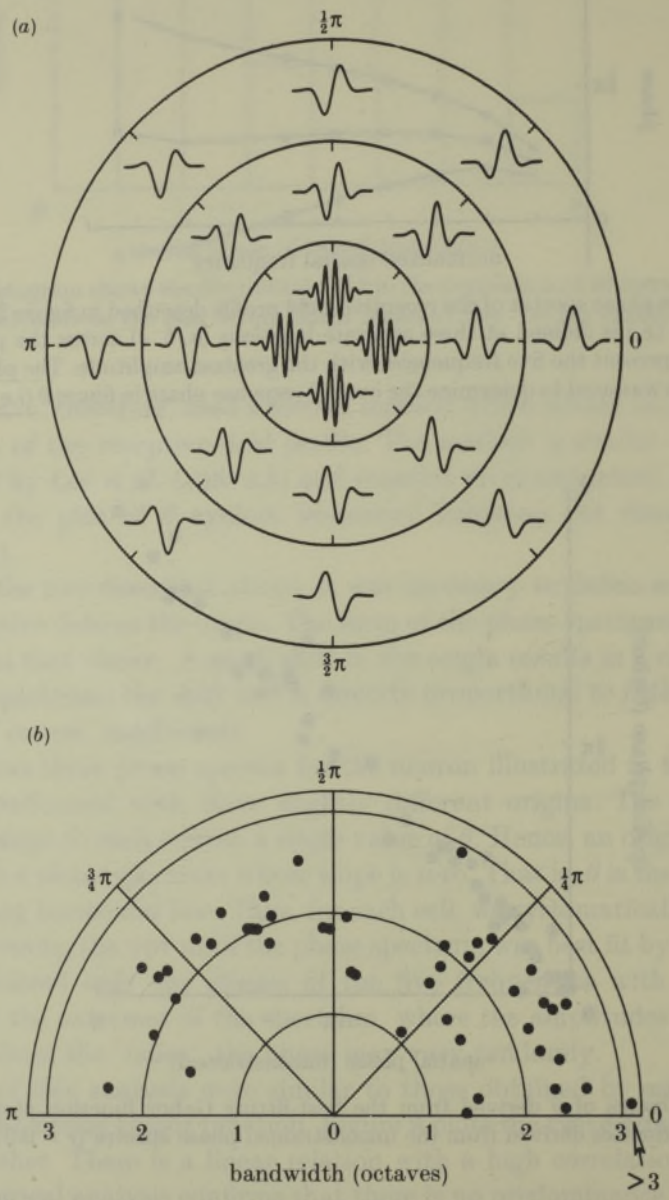

FIGURE 10. (*a*) Polar plot of several Gabor functions that have the same envelope width (σ). Phase (θ) is plotted as the angle from horizontal and the period of the carrier frequency ($1/f$) increases with the distance from the origin. Using the bandwidth measure derived in (7), we plot Gabor functions with bandwidths of 0.5, 1.5 and 2.5 octaves. (*b*) Results for the 46 cells based on the best-fitting Gabor function. Again, bandwidth is derived from equation 5. Only the range of 0 to π is represented because the complete range of phases is confounded by the variety of preferred orientations. See text for details.

frequency ($1/f$) increases with the distance from the origin. With the exception of overall size, this plot is a complete representation of possible Gabor functions. Each function is represented by a unique point on such a plot. Because we have shown previously (figure 6) that our receptive-field profiles are well fit by Gabor functions, such a plot should provide a thorough description of the variety of shapes found with simple cells receptive field profiles.

The amplitude spectra of functions near the centre of such a plot will have narrow spatial-frequency bandwidths. If the envelope width is held constant, then increasing the period of the carrier frequency will increase the bandwidth.

Kulikowski *et al.* (1982) have shown that the bandwidth in octaves (B) can be related to the envelope width (σ) and carrier frequency (f) according to the following equation:

$$B = \log_2[(1+0.1874/R)/(1-0.1874/R)], \tag{7}$$

where R is the envelope width divided by the optimal frequency ($R = \sigma/f$). The advantage of this method of estimating bandwidth is that it is not confounded by the symmetry of the profile (see Appendix 2), and it also obviates the difficulty of measuring from amplitude spectra that lack a sufficient low-frequency cut.

In figure 10*a*, f is varied such that the bandwidth increases linearly with the distance from the origin. Gabor functions with 0.5, 1.5, and 2.5 octave bandwidths are shown. As one can see, for functions with narrow bandwidths (e.g. 0.5 octaves), a change in phase (θ) produces little change in the function's profile. Indeed, a little noise is likely to have much more effect on the estimated symmetry if the receptive-field profile has a narrow bandwidth.

If our non-symmetric profiles (i.e. neither even nor odd symmetric) were relatively narrow-band, then it might be possible to maintain the notion that 'phase-selective' profiles are even and odd symmetric.

The results of this analysis are shown in figure 10*b*. All points are based on the best-fitting Gabor function described above. Again, because we are involved with cells with a variety of preferred orientations, the results must only reflect phase-selectivity between 0 and π. As in figure 10*a*, this is a polar plot, where bandwidth in octaves is measured as the distance from the origin. Response phase is measured as the angle from horizontal.

The results in figure 10*b* show no systematic relation between bandwidth and phase.

Discussion

It is certainly convenient to assume that simple cell receptive-field profiles are described by Gabor functions. In terms of modelling the visual system, such functions are easily calculated and manipulated. Furthermore, they seem to be theoretically ideal for conveying information about *both* spatial position *and* spatial frequency (Gabor 1946). Within this framework, it is also convenient to assume that the profiles have only two general shapes; even and odd symmetric.

To test these popular assumptions, we have performed a quantitative analysis

on the structure of simple-cell receptive-field profiles of cats. With regard to the one-dimensional structure of these profiles as derived from the line-weighting functions, there are two main conclusions:

1. to a first approximation, the receptive-field profiles *can* indeed be described as Gabor functions;

2. however, the receptive-field profiles of these cells do *not* fit into even- and odd-symmetric categories.

As shown in figure 10*a*, there is a large variety of theoretical Gabor functions. Indeed, one might think that almost any conceivable receptive-field profile could be fit by a Gabor function of some kind. It may therefore be worthwhile to ask what types of receptive fields are rejected by this analysis. Figure 11 shows four hypothetical receptive-field profiles which cannot be described by Gabor functions. The envelopes are not even approximately Gaussian. There is no *a priori* reason to assume that the receptive-field profiles cannot take on these forms, but our results suggest that such profiles are at least unlikely.

One should note that we are not arguing that a Gabor function necessarily provides the best possible fit to all our data. Indeed, other functions which provide more degrees of freedom might well provide a better fit. The advantage of the Gabor function is partly due to its effectiveness in providing a good account of the data with only three free parameters (four if one includes amplitude). However, as shown in figure 11, the analysis in terms of Gabor functions also provides insight into the types of profile that are *not* found.

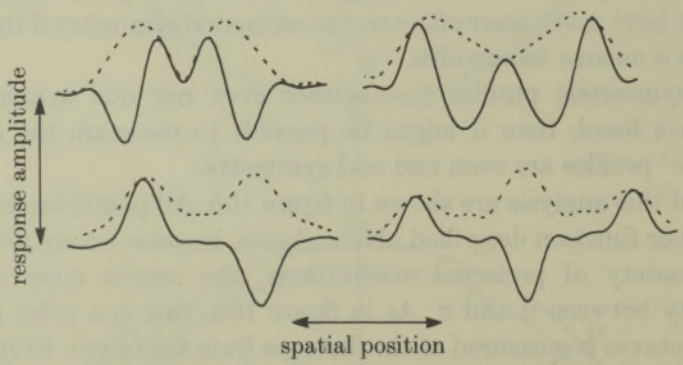

FIGURE 11. Some hypothetical receptive field profiles (solid lines) which do *not* fit into the Gabor function analogy. Also shown are their respective envelopes (dashed lines).

Do these results provide us with some insight into the functional significance of these cells? If receptive fields are Gabor functions, then they are ideally suited for encoding the spatial frequency and position of a signal. It has been suggested that this may be 'why' the receptive fields are shaped this way (Marcelja 1980). However, without clues as to how the information from the cells is processed, such conclusions can be no more than speculation. That is, any answers about what a simple cell codes for, must involve an analysis of how the later stages of the visual system deal with the information conveyed by simple cells. One cannot rule out the possibilities that these theoretically attractive shapes reflect just the limitations

in the spread of the dendritic fields or just some general rules about how the input from the lateral geniculate nucleus can be combined. The data at hand are simply insufficient to answer general questions about the 'visual code'.

However, for those models of visual processing which have assumed that simple cells can be described as Gabor functions (see, for example, Sakitt & Barlow 1982; Kulikowski *et al.* 1982; Watson 1983), these results can be taken as some measure of support. Our data, at the very least, are consistent with such an hypothesis.

Our second conclusion opposes the suggestions of several investigators that the simple-cell receptive fields fall at least roughly into even- and odd-symmetric categories (Movshon *et al.* 1978; Kulikowski & Bishop 1981*a*,*b*; Pollen & Ronner 1981; Maske *et al.* 1985). Figure 10*b* shows that our results do not support this suggestion. In this plot, if the cells were even symmetric the data would fall along angles corresponding to 0 and π. If the cells were odd symmetric, then the data would lie at $\frac{1}{2}\pi$. Clearly, the data do not fall into these groups.

Why should our results differ from the suggestions of these previous investigators? First, we should point out that these investigators have noted that the cells only 'appear' to be even or odd symmetric. None of these investigators performed any quantitative analysis of the receptive fields. We would expect that such an analysis on their data would support our view (indeed, the data described by Movshon *et al.* are part of the present data set).

Secondly, there seems to be some misconception about the basis functions that are necessary for a theoretically 'complete' analysis by a computational system. Investigators have used even- and odd-symmetric mechanisms centred at the same point in space to serve as the basis functions for each orientation, position and frequency (Kulikowski *et al.* 1982; Sakitt & Barlow 1982; Watson 1983). Although such mechanisms may be sufficient, they are by no means necessary. As Gabor points out, the two functions need only differ in phase by $\frac{1}{2}\pi$.

Pollen & Ronner (1981) found that adjacent simple cells are often tuned to the same orientation and spatial frequency and differ in phase by about 90° ($\frac{1}{2}\pi$) across the different spatial frequencies tested. They state that the receptive fields of these pairs of cells 'must be conjugate pairs, that is, one field with even symmetry and one with odd symmetry around the same axis.' Although they noted that line-weighting functions of two pairs of such cells looked 'approximately' even and odd symmetric, their data only supports the notion that adjacent simple cell profiles are 'in quadrature' (Gabor 1946). That is, they have phase spectra that differ by $\frac{1}{2}\pi$. This is still an exciting finding since it suggests that adjacent cells may serve as adequate basis functions. However, their results are not inconsistent with ours. It may be that pairs of adjacent cells differ by $\frac{1}{2}\pi$ but appear in a variety of different forms (e.g. $\frac{1}{4}\pi$–$\frac{3}{4}\pi$ and $\frac{1}{8}\pi$–$\frac{5}{8}\pi$).

However, we must allow for the possibility that the differences in our conclusions are due to the differences in our methods. All the receptive fields reported here were mapped with stationary lines. Maske *et al.* (1985), on the other hand, mapped their receptive fields with moving lines. Although the responses to moving lines are confounded by the temporal characteristics of the response, they suggest that the moving lines can reveal sub-regions that stationary lines will not. It has also

been suggested (Andrews & Pollen 1979; Kulikowski & Bishop 1981*a*; Glezer *et al.* 1982) that sinusoidal gratings will imply the existence of more receptive field subregions than are actually found with stationary lines.

It must be pointed out that the estimated bandwidths of our cells as determined from the best-fitting Gabor function (figure 10), are relatively broad. The bandwidths range from about 1.5–2.5 octaves. Studies that derive estimates directly from the responses to moving sinusoidal gratings find narrower bandwidths than this (Movshon *et al.* 1978; Tolhurst & Thompson 1981). Kulikowski & Bishop (1981*b*) suggest that this disparity between the two methods provides further support for the notion that flashed bars reveal fewer flanking subregions than do moving bars or gratings.

Thus we must accept the notion that the receptive field profile, predicted by transformation of the spatial frequency response, is not a perfect match to the profile measured directly with stationary lines. It may be that this reflects some gross nonlinearity of spatial summation (Tolhurst & Dean 1986). Or, it may simply be that the responses of some parts of the receptive field are too small to exceed threshold when presented with narrow lines. Perhaps, more 'complete' receptive-field profiles would show a greater degree of even and odd symmetry. Although we consider this last possibility to be unlikely, it does suggest a degree of caution when generalizing our conclusions.

Finally, let us consider what effect these results might have on general theories of visual processing. We noted that our results are consistent with models that describe simple cells as Gabor functions. However, the results are not consistent with models that assume that the receptive fields are either even or odd symmetric (Marcelja 1980; Kulikowski *et al.* 1982; Sakitt & Barlow 1982; Watson 1983). Even the authors of this paper have proposed such models to account for their psychophysical data (Tolhurst & Dealy 1975; Field & Nachmias 1984).

It is not clear how such models must be modified to take account of our findings. The variety of receptive field types appears to add a measure of complexity to any overall description of the role of simple cells in general visual processing. Indeed, theories that suggest that each receptive field type carries a 'labelled line', may find our results especially troublesome because we have added to the number of necessary labels.

We thank Professor F. W. Campbell and Dr L. Ling for their helpful advice and criticism. The experiments were performed in collaborative experiments between D.J.T. and J. A. Movshon, I. D. Thompson and A. F. Dean. We are grateful to them for their contributions. The experiments were supported by the Medical Research Council and the Wellcome trust. D.J.F. was supported by a National Eye Institute Research Fellowship Award F32 EY05737-01.

Appendix 1

The estimated receptive-field profile (as derived from the discrete Fourier transform) is subject to three potential sources of error. The extent of this error is primarily dependent on the amount of energy beyond the frequency at which

the spectrum is truncated. Because the amplitude spectra were approaching zero for most cells, the magnitude of this error is expected to be minor. None the less, we describe these errors below and provide an example of the effects of these errors on a hypothetical receptive-field profile (figure 12).

1. The most significant error introduced by the DFT usually involves the effects of removing frequencies beyond the cutoff frequency (i.e. half the sampling frequency). For a continuous function, this can introduce a 'ripple' across the spatial extent of the function. The magnitude of this ripple will be dependent on the amplitude of the spectrum at the cutoff frequency.

2. The spectrum of a single bar is not flat, but falls off with increasing frequency according to

$$A(f) = \sin(\pi fW)/(\pi fW),$$

where W is the width of the bar. In other words, the spectrum as derived with these bars will fall below that of the actual spectrum of the profile. For example, at the cutoff frequency of the DFT (i.e. $f = 0.5/W$) the amplitude of the derived spectrum may be only 65 % of the actual spectrum.

3. Frequencies higher than the cutoff frequency may be 'aliased' by the sampling positions of the bars and reflect back onto the spectrum. Thus the derived spectra may not perfectly represent the actual spectra of the cells. The effect of this aliasing is expected to be minimal for two reasons. First, for most profiles, there is likely to be little energy beyond the cutoff frequency and hence little energy that might be aliased. Second, because the spectrum of a bar falls off at higher frequencies (see point 2), the response to any aliasing frequencies is also reduced. That is, the response to a bar is not determined by a single point along the profile, but by the entire region corresponding to the width of the bar. By integrating across the width of the bar, the aliasing of higher frequencies is greatly reduced.

Figure 12 shows how these three errors can affect the estimated receptive-field

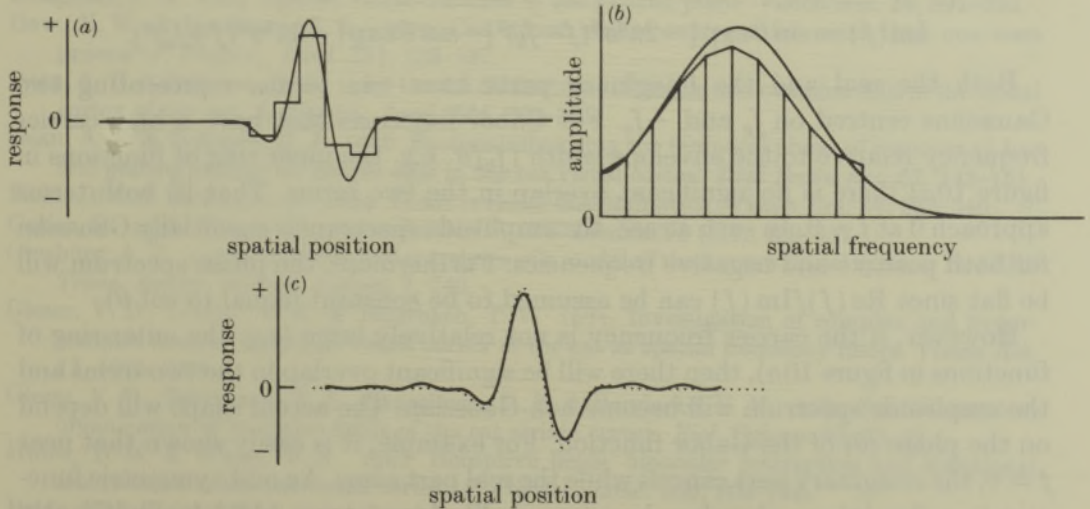

FIGURE 12. The discrete Fourier transform applied to a hypothetical receptive-field profile. See text.

profile of a hypothetical cell. In this example we have intentionally chosen a bar width which is large relative to the size of the profile. Figure 12*a* shows the hypothetical profile (smooth curve) along with the theoretical response to a series of bars at the positions shown. The response to each bar is determined by integrating the area of the profile under the bar. Figure 12*b* shows the actual amplitude spectrum of the profile (smooth curve) along with the spectrum derived from the DFT. For much of the spectrum, one can see that the DFT amplitude spectrum falls below that of the actual spectrum in agreement with point 2 above. However, at the highest frequencies of the DFT, the effect is reversed. This relative rise in the spectrum is a result of the aliasing of those frequencies above the cutoff frequency. Figure 12*c* shows the original hypothetical profile (dotted line) along with the profile as derived from the DFT (solid line). One can see that, although the two profiles differ, the basic form of the profile is relatively unchanged. Indeed, even with a significant proportion of the spectrum removed, the phase of this estimated profile differs from that of the original by less than 0.095 rad (5.4°).

Thus the receptive-field profile, as estimated from the discrete Fourier transform, is not a perfect representation of the original profile. However, considering that the magnitude of this error is small relative to the variation between cells, the conclusions drawn from these data should remain unaffected.

Appendix 2

Consider a Gabor function which follows

$$R(x) = k \exp[-x^2/2\sigma^2] \cos(2\pi f_0 x - \theta),$$

where $k = 1/(\sigma\sqrt{(2\pi)})$.

The Fourier transform has a real part

$$\mathrm{Re}(f) = \cos\theta \exp[-2\pi^2\sigma^2(f-f_0)^2] + \cos\theta \exp[-2\pi^2\sigma^2(f+f_0)^2]$$

and an imaginary part

$$\mathrm{Im}(f) = \sin\theta \exp[-2\pi^2\sigma^2(f-f_0)^2] - \sin\theta \exp[-2\pi^2\sigma^2(f+f_0)^2].$$

Both the real and the imaginary parts have two terms, representing two Gaussians centred on f_0 and $-f_0$. For Gabor functions that have a high carrier frequency relative to the envelope width (f_0/σ, e.g. the inner ring of functions in figure 10*a*) there is no significant overlap in the two terms. That is, both terms approach 0 at $f = 0$. In such a case, the amplitude spectrum is essentially Gaussian for both positive and negative frequencies. Furthermore, the phase spectrum will be flat since $\mathrm{Re}(f)/\mathrm{Im}(f)$ can be assumed to be constant (equal to $\cot\theta$).

However, if the carrier frequency is not relatively large (e.g. the outer ring of functions in figure 10*a*), then there will be significant overlap in the two terms and the amplitude spectrum will become non-Gaussian. The actual shape will depend on the phase (θ) of the Gabor function. For example, it is easily shown that near $f = 0$, the imaginary part cancels while the real part sums. An odd-symmetric function (e.g. $\theta = \frac{1}{2}\pi$) can therefore have an amplitude spectrum which is significantly different from that of an even-symmetric function (e.g. $\theta = 0$) even though the carrier frequency (f_0) and the envelope width (σ) are unchanged.

Further, the phase spectrum will not be flat. For a function that has both real and imaginary parts (e.g. $\theta = \frac{1}{4}\pi$), the low frequencies will be primarily real (i.e. cosine) because in this region the imaginary part cancels and the real part sums. Therefore, at low frequencies, the phase spectrum will shift towards $\theta = 0$ for functions having a carrier phase between 0 and $\frac{1}{2}\pi$. For functions having a carrier between $\frac{1}{2}\pi$ and π, the spectrum will shift towards $\theta = \pi$.

There are two consequences for Gabor functions with relatively low carrier frequencies. First, if the spatial frequency bandwidth of the Gabor function is estimated from the amplitude spectrum, then the bandwidth will be confounded by the response phase. (This is not the case if bandwidth is defined in relation to the envelope width and carrier frequency, e.g. figure 10.) Second, because the phase spectra are not flat, the Hilbert transforms of these Gabor functions will not be Gabor functions shifted by $\frac{1}{2}\pi$. Hence, the derived envelope (figure 3) will not be strictly Gaussian.

References

Andrews, B. W. & Pollen, D. A. 1979 Relationship between spatial frequency selectivity and receptive field profile of simple cells. *J. Physiol., Lond.* **287**, 163–176.

Albrecht, D. G., DeValois, R. L. & Thorell, R. G. 1979 Visual cortical neurons: are bars or gratings the optimal stimuli? *Science, N.Y.* **207**, 88–90.

Blakemore, C. & Campbell, F. W. 1969 On the existence of neurones in the human visual system selectively sensitive to the orientation and size of retinal images *J. Physiol., Lond.* **203**, 237–260.

Bracewell, R. N. 1965 *The Fourier transform and its applications*. New York: McGraw-Hill.

Campbell, F. W., Cooper, G. F. & Enroth-Cugell, C. 1969 The spatial selectivity of the visual cells of the cat. *J. Physiol., Lond.* **203**, 223–235.

Campbell, F. W. & Robson, J. G. 1968 Application of Fourier analysis to the visibility of gratings. *J. Physiol., Lond.* **197**, 551–566.

Cooper, G. F. & Robson, J. G. 1968 Successive transformations of spatial information in the visual system. In *I.E.E. N.P.L. Conf. Proc.* **42**, 134–143. London: I.E.E.

Daugman, J. G. 1984 Spatial visual channels in the Fourier plane. *Vision Res.* **24**, 891–910.

Daw, N. W. & Pearlman, A. L. 1970 Cat colour vision: evidence for more than one cone process. *J. Physiol., Lond.* **211**, 125–137.

Dean, A. F. & Tolhurst, D. J. 1983 On the distinctness of simple and complex cells in the visual cortex of the cat. *J. Physiol., Lond.* **344**, 305–325.

Dean, A. F. & Tolhurst, D. J. 1986 Factors influencing the temporal phase of response to bar and grating stimuli for simple cells in the cat visual cortex. *Expl Brain Res.* **62**, 143–151.

Field, D. J. & Nachmias, J. 1984 Phase reversal discrimination. *Vision Res.* **24**, 333–340.

Gabor, D. 1946 Theory of communication *J. IEE London.* **93** (III), 429–457.

Ginsburg, A. P. 1971 Psychological correlates of a model of the human visual system. In *IEEE Trans. Aerosp. electron. systems* **7**, 740.

Glezer, V. D., Ivanov, V. A. & Tsherbach, T. V. 1973 Investigation of complex and hypercomplex receptive fields of visual cortex of the cat as spatial frequency filters. *Vision Res.* **13**, 1875–1904.

Glezer, V. D., Tsherbach, T. A., Gauselman, V. E. & Bondarko, V. M. 1982 Spatio-temporal organization of receptive fields of the cat striate cortex. *Biol. Cybern.* **43**, 35–49.

Hubel, D. H. & Wiesel, T. N. 1962 Receptive fields, binocular interaction and functional architecture in the cat visual cortex. *J. Physiol., Lond.* **160**, 106–154.

Ikeda, H. & Wright, M. J. 1975 Spatial and temporal properties of 'sustained' and 'transient' cortical neurons in area 17 of the cat. *Expl Brain Res.* **22**, 363–383.

Kulikowski, J. J. & Bishop, P. O. 1981*a* Fourier analysis and spatial representation in the cat visual cortex. *Experientia* **37**, 160–163.

Kulikowski, J. J. & Bishop, P. O. 1981*b* Linear analysis of the responses of simple cells in the cat visual cortex. *Expl Brain Res.* **44**, 386–400.

Kulikowski, J. J. & King-Smith, P. E. 1973 Spatial arrangement of line, edge and grating detectors revealed by subthreshold summation. *Vision Res.* **13**, 1455–1478.

Kulikowski, J. J., Marcelja, S. & Bishop, P. O. 1982 Theory of spatial position and spatial frequency relations in the receptive fields of simple cells in the cat visual cortex. *Biol. Cybern.* **43**, 187–198.

Lee, B. B., Elepfandt, A. & Virsu, A. 1981*a* Phase of responses to moving sinusoidal gratings in cells of cat retina and lateral geniculate nucleus. *J. Neurophysiol.* **45**, 807–817.

Lee, B. B., Elepfandt, A. & Virsu, A. 1981*b* Phase of responses to sinusoidal gratings in cat striate cortex. *J. Neurophysiol.* **45**, 818–828.

Levick, W. R. 1972 Another tungsten microelectrode *Med. biol. Engng* **10**, 510–515.

Maffei, L. & Fiorentini, A. 1973 The visual cortex as a spatial frequency analyzer. *Vision Res.* **13**, 1255–1268.

Marcelja, S. 1980 Mathematical description of the responses of simple cortical cells. *J. opt. Soc. Am.* **70**, 1297–1300.

Maske, R., Yamene, S. & Bishop, P. O. 1985 Simple and B-cells in cat striate cortex. Complementarity of responses to moving light and dark bars. *J. Neurophysiol.* **53**, 670–685.

Merrill, E. G. & Ainsworth, A. 1972 Glass-coated platinum-plated tungsten microelectrodes. *Med. biol. Engng* **10**, 662–672.

Movshon, J. A., Thompson, & Tolhurst, D. J. 1978 Spatial summation in the receptive fields of simple cells in the cat's striate cortex. *J. Physiol.* **283**, 53–77.

Palmer, L. A., Jones, J. P. & Mullikin, W. H. 1985 Functional organization of simple cell receptive fields. In *Models of the visual cortex* (ed. D. Rose and V. G. Dobson), pp. 273–280. New York: Wiley.

Pollen, D. A. & Ronner, S. F. 1981 Phase relationships between adjacent simple cells in the cat. *Science, N.Y.* **212**, 1409–1411.

Robson, J. G. 1980 Neural images: the physiological basis of spatial vision. In *Visual coding and adaptability* (ed. C. S. Harris), pp. 177–214. Hillsdale, New Jersey: Lawrence Erlbaum Associates.

Sakitt, B. & Barlow, H. B. 1982 A model for the economical encoding of the visual image in cerebral cortex. *Biol. Cybern.* **43**, 97–108.

Tolhurst, D. J. & Dean, A. F. 1986 Spatial summation by simple cells in the striate cortex of the cat. *Expl Brain Res.* (In the press.)

Tolhurst, D. J. & Dealy, R. S. 1975 The detection and identification of lines and edges. *Vision Res.* **15**, 1367–1372.

Tolhurst, D. J. & Thompson, I. D. 1982 On the variety of spatial frequency selectivities shown by neurons in area 17 of the cat. *Proc. R. Soc. Lond.* B **213**, 183–199.

Watson, A. B. 1983 Detection and recognition of simple spatial forms. In *Physical and biological processing of images* (ed. O. J. Braddick and A. C. Slade), pp. 100–114. Berlin: Springer-Verlag.

de Weerd, J. P. C. & Kap, J. I. 1981 Spectro-temporal representations and time-varying spectra of evoked potentials. *Biol. Cybern.* **41**, 101–117.

Weisstein, N. & Bisaha, J. 1972 Gratings mask bars and bars mask gratings: visual frequency response to aperiodic stimuli. *Science, N.Y.* **176**, 1047–1049.